

Remarkable site selectivity properties of the ARPES matrix element in $\text{Bi}_2\text{Sr}_2\text{CaCu}_2\text{O}_8$

S. Sahrakorpi¹, M. Lindroos^{1,2} and A. Bansil¹

¹*Physics Department, Northeastern University, Boston, Massachusetts 02115*

²*Institute of Physics, Tampere University of Technology, P.O. Box 692, 33101 Tampere, Finland*

(Dated: November 20, 2018)

We show that the ARPES spectra for emission from the bonding as well as the antibonding Fermi surface sheet in $\text{Bi}_2\text{Sr}_2\text{CaCu}_2\text{O}_8$ (Bi2212) possess remarkable site selectivity properties in that the emission for photon energies less than 25 eV is dominated by $p \rightarrow d$ excitations from just the O-sites in the CuO_2 planes. There is little contribution from Cu electrons to the ARPES intensity, even though the initial states at the Fermi energy contain an admixture of Cu- d and O- p electrons. We analyze the origin of this effect by considering the nature of the associated dipole matrix element in detail and find that various possible transition channels (other than $p \rightarrow d$ on O-sites) are effectively blocked by either the fact that the related radial cross section is small and/or a lack of available final states. Our prediction that ARPES can preferentially sample Cu or O states by tuning the photon energy suggests novel possibilities for exploiting energy dependent ARPES spectra for probing initial state characters in the cuprates.

PACS numbers: 79.60.bm, 71.18.+y, 74.72.Hs

I. INTRODUCTION

The photointensity observed in an angle-resolved photoemission (ARPES) experiment is the result of modulation of the spectral density of the initial state via the ARPES matrix element. This modulation can be quite substantial in the cuprates and depends in general strongly on \mathbf{k}_{\parallel} , polarization and energy of the incident photons as well as the energy and character of the initial state.^{1,2,3,4,5,6,7,8,9} Chuang et al.⁵, for example, have recently exploited the large theoretically predicted differences in the ARPES cross sections of bonding and antibonding pieces of the Fermi surface (FS) by tuning the photon energy to adduce the doping dependence of the bilayer splitting in $\text{Bi}_2\text{Sr}_2\text{CaCu}_2\text{O}_8$ (Bi2212). Asensio et al.⁴ find that apparently different looking Fermi surface maps obtained in Bi2212 over wide area in the $(\mathbf{k}_x, \mathbf{k}_y)$ plane at different photon energies largely reflect the effect of the ARPES matrix element. In other applications, such as a recent proposal¹⁰ to determine the spectral function of the boson mediating the Cooper pairs in the cuprates, it will be necessary to develop strategies for minimizing the effect of the ARPES matrix element in order to obtain robust physical results through ARPES spectra. It is clear that a good understanding of the nature of the ARPES matrix element is of considerable importance in continued development of ARPES as a probe of electronic structure of complex materials.

With this motivation, we examine in this article the nature of emissions from the bonding as well as the antibonding parts of the FS of Bi2212. In considering contributions to photointensity arising from different angular momentum channels and various atomic sites in the unit cell, we find that the ARPES matrix element possesses remarkable site selectivity properties in that the ARPES intensity throughout the $(\mathbf{k}_x, \mathbf{k}_y)$ plane in the 5-25 eV energy range is dominated by only the O $p \rightarrow d$ tran-

sitions. The contribution from Cu sites is quite small, even though the electronic states at the Fermi energy in Bi2212 contain substantial Cu character. In order to ascertain the origin of this effect, the dipole transition matrix element between the relevant initial and final states is analyzed in detail and the factors responsible for this behavior are identified.²⁷ Our prediction that ARPES can preferentially sample Cu or O states suggests novel possibilities for exploiting energy dependent ARPES spectra to gain insight into character of initial states in complex materials.

The paper is ordered as follows. In Section II we briefly discuss the underlying formalism. Section III presents and analyzes the nature of the ARPES spectra. In Subsection IIIA, a typical ARPES spectrum for emission from the Fermi energy in Bi2212 is considered to orient the reader. Subsection IIIB continues with a discussion of site-resolved photointensities over the 5-25 eV photon energy range for \mathbf{k}_{\parallel} values covering the entire $(\mathbf{k}_x, \mathbf{k}_y)$ plane. The origin of the site-selectivity effect is then delineated in Subsection IIIC. Finally, Section IV makes some concluding remarks, including possible application of site-selectivity property in gaining insight into interesting issues such as the Zhang-Rice mechanism^{11,12} in the cuprates and the doping dependence of the Hubbard U parameter via energy dependent ARPES measurements¹³.

II. OVERVIEW OF FORMALISM

The methodology used in this study has been discussed previously in Ref. 2, to which we refer the reader for details; See also Refs. 1,14,15,16,17,18,19. Some comment in this connection is nevertheless necessary in order to meaningfully describe the new results presented here. In particular, Ref. 2 shows that substantial insight into the

nature of the ARPES photointensity²⁸ resulting from excitation between specific bulk initial and final states in the solid, $\tilde{\psi}_i$ and $\tilde{\psi}_f$, can be obtained in terms of the behavior of the corresponding momentum matrix element, $\langle \tilde{\psi}_f | \mathbf{p} | \tilde{\psi}_i \rangle$. We then expand the $\tilde{\psi}$ within the KKR band structure scheme^{20,21} as

$$\tilde{\psi}(\mathbf{r}) = \sum_{L,\beta} i^l C_L^\beta R_l^\beta(r) Y_L(\Omega), \quad (1)$$

where $L \equiv (l, m)$ is a composite angular momentum index, $Y_L(\Omega)$ are real spherical harmonics and β denotes different basis sites. C_L^β are expansion coefficients and $R_l^\beta(r)$ is the radial part of the Bloch wave function on site β . The use of form (1) for the initial and final states yields^{2,18,19,22}

$$\langle \tilde{\psi}_f | \mathbf{p} | \tilde{\psi}_i \rangle = \sum_{\alpha,\beta} \sum_{L,L'} \hat{\mathbf{e}}_\alpha i^{l-l'-1} C_{L'}^{\beta*} C_L^\beta B_{l,l'}^\beta \mathcal{G}_{L,L'}^\alpha. \quad (2)$$

Here $\hat{\mathbf{e}}_\alpha$ denotes a unit vector along α -direction and primed indices refer to the final state. $\mathcal{G}_{L,L'}^\alpha$ are the standard Gaunt coefficients. The detailed expression for $B_{l,l'}^\beta$ is given in Ref. 2. For present purposes, the important point to recognize is that

$$B_{l,l'}^\beta \propto \int_0^{r_{MT}^\beta} R_{l'}^\beta(r)^* r R_l^\beta(r) r^2 dr, \quad (3)$$

where the integral extends to the muffin-tin radius r_{MT}^β of the atom β in the basis. It is useful to decompose the momentum matrix element into contributions from various angular momentum channels and sites in the unit cell as follows:

$$M_\alpha \equiv \langle \tilde{\psi}_f | p_\alpha | \tilde{\psi}_i \rangle = \sum_\gamma M_\alpha^\gamma \quad (4)$$

$$= \sum_\gamma \sum_{L,L'} M_{\alpha,L,L'}^\gamma, \quad (5)$$

with

$$M_{\alpha,L,L'}^\gamma = \sum_\delta i^{l-l'-1} (C_{L'}^{\gamma,\delta})^* C_L^{\gamma,\delta} B_{l,l'}^{\gamma,\delta} \mathcal{G}_{L,L'}^\alpha. \quad (6)$$

Aside from the obvious notation in Eqs. 4-6, indices γ and δ are together meant to encompass the summation of Eq. 2 over all basis sites β in the unit cell. In the present case of tetragonal Bi2212, γ takes on eight distinct values which include the Ca atom and seven pairs of symmetrically located atoms (Bi, O_{Bi} , Sr, O_{Sr} , Cu, $O_{Cu,x}$, $O_{Cu,y}$). δ in Eq. 6, on the other hand, takes only two values, which account for the two atoms placed symmetrically with respect to the Ca layer in the unit cell. In this sense, we may think of γ as a ‘‘site’’ index and δ as a ‘‘pairing’’ index. In this work we study particularly the matrix element $M_{\alpha,L,L'}^\gamma$, which includes the contribution of pairs of sites δ related by mirror symmetry. We will see that its dependence on different sites and excitation

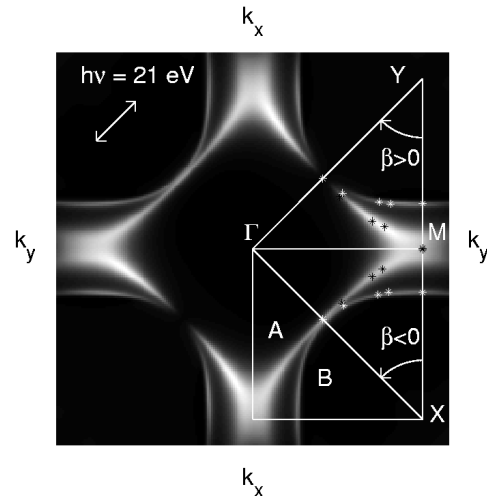


FIG. 1: Grey scale plot (white denotes high) of theoretical ARPES intensity for emission from the Fermi energy at $h\nu = 21$ eV for tetragonal Bi2212. Light is assumed to be polarized along $[110]$ (white arrow). White and black stars give the \mathbf{k}_{\parallel} -points (corresponding to different angles β) where the energy dependence of the dipole matrix element for the bonding (B) and antibonding (A) Fermi surface sheets shown in Figs. 2 and 3 has been computed.

channels $L \rightarrow L'$ is important for delineating the nature of photointensity in Bi2212.

Concerning relevant computational details, the crystal potential used is the same as that employed in our previous studies of Bi2212 on a body centered tetragonal lattice and involves 30 atoms per unit cell; See, e.g., Refs. 1 and 2. For definiteness, incident light is assumed polarized along the $[110]$ -direction. The damping of final states is included via an imaginary part of the final state self-energy, $\Sigma_f'' = 2$ eV. In order to understand the \mathbf{k}_{\parallel} and energy dependencies of the dipole matrix element, calculations were carried out over the photon energy range of 5-25 eV for each of the 20 \mathbf{k}_{\parallel} -points considered in the $(\mathbf{k}_x, \mathbf{k}_y)$ -plane. This set of \mathbf{k}_{\parallel} -points covers both the bonding and the antibonding parts of the bilayer split Fermi surface of Bi2212.

III. RESULTS

A. ARPES spectrum of Bi2212

For orientation, Fig. 1 shows a typical computed one-step ARPES spectrum for emission from the E_F at 21 eV. The Umklapp and shadow features^{3,4} are not included in this simulation for simplicity. The imprints of the bilayer-split bonding (B) and antibonding (A) parts of the FS are seen clearly and are in remarkable accord with recent ARPES experiments^{3,4,5,7,23}. The bonding band gives

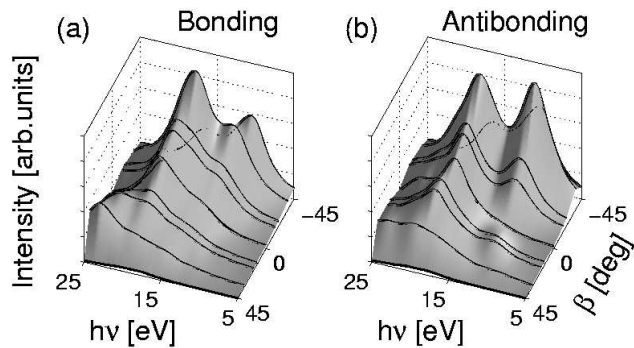


FIG. 2: Intensity \tilde{I} (Eq. 7) for \mathbf{k}_{\parallel} -points (given by the angle β of Fig. 1) lying along the bonding and antibonding Fermi surface sheets in tetragonal Bi2212 over the photon energy range of $h\nu = 5 - 25$ eV. Intensities have been smoothed to reflect final state damping effect. Results in (a) and (b) are not normalized in relation to each other.

rise to the X (Y) centered hole sheet B. The antibonding band is responsible for the electron-like Γ -centered sheet A with a very narrow neck around the M -point². The associated intensity appears somewhat diffuse due in part to the presence of a van Hove singularity in the electronic spectrum close to M . Note that the polarization vector of the incident light (white arrow) breaks the symmetry between the irreducible regions $\Gamma - Y - M$ and $\Gamma - M - X$ of the Brillouin zone. For this reason, we have characterized the \mathbf{k} -points on the A and B FS's in these two regions by the indicated angle β , where $\beta > 0$ refers to the upper half and $\beta < 0$ to the lower half on the right hand side of the figure. The intensity from either the A or the B sheet is zero along the nodal line $\Gamma - Y$ ($\beta = 45^\circ$), but this is not the case for the symmetrically placed nodal line $\Gamma - X$ for $\beta = -45^\circ$. This is due to the fact that even though the momentum matrix elements M_x and M_y are non-zero in general they add (for the present polarization) destructively along $\Gamma - Y$ but constructively along the $\Gamma - X$ line.

As already noted, insight into the ARPES intensity can be obtained by considering the momentum matrix element $\langle \tilde{\psi}_f | \mathbf{p} | \tilde{\psi}_i \rangle$ which connects the relevant initial and final states and the associated intensity

$$\tilde{I} = |\mathbf{A} \cdot \langle \tilde{\psi}_f | \mathbf{p} | \tilde{\psi}_i \rangle|^2. \quad (7)$$

Fig. 2 shows intensity computed by using Eq. 7 for a series of \mathbf{k}_{\parallel} -points lying along the bonding and antibonding Fermi surface sheets characterized by the angle β of Fig. 1. It is clear that the dipole matrix element varies strongly with photon energy and \mathbf{k}_{\parallel} . The main features in the intensity from both the bonding and antibonding bands are the two peaks at $h\nu$ around 11 eV and 18 eV.

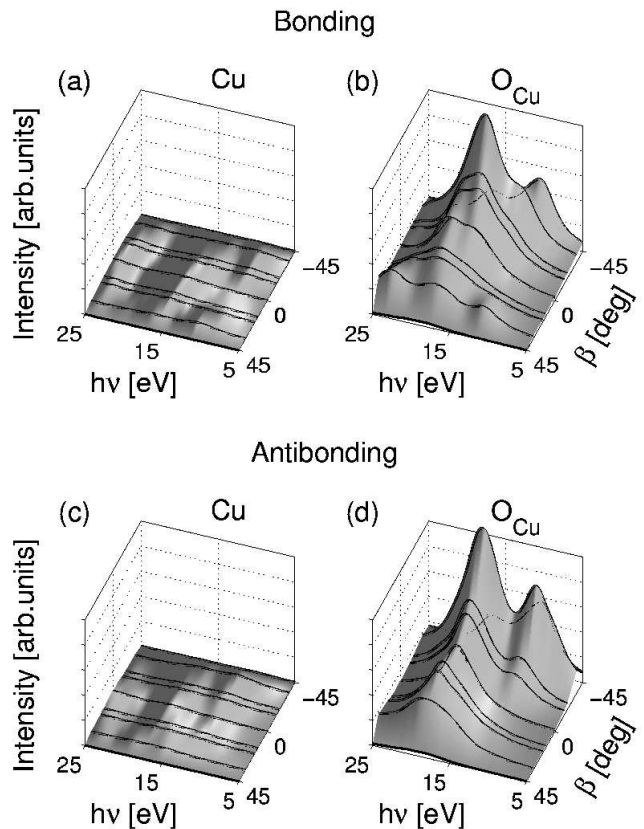


FIG. 3: Contributions to the photointensities of Fig. 2 from Cu and O sites in the CuO_2 planes in the crystal lattice. (a) and (c) give contribution from Cu sites for transitions from the bonding and the antibonding initial states respectively. (b) and (d) similarly refer to the O-sites. See caption to Fig. 2 for other details.

B. Contributions to photointensity from different sites

We next consider the extent to which Cu and O related initial state electrons are excited in the photoemission process. Fig. 3 gives site (γ) resolved contributions to the photointensities obtained by taking into account only the terms related to Cu or O_{Cu} -sites of the CuO_2 planes, i.e. for $\gamma \equiv \text{Cu}$ or $\gamma \equiv \text{O}_{\text{Cu},x} + \text{O}_{\text{Cu},y}$ in Eq. 4, where the corresponding contributions from the two CuO_2 planes are added together. Fig. 3(a) shows the Cu contribution from the bonding initial state as a function of \mathbf{k}_{\parallel} and photon energy. The intensity is seen to be practically zero indicating that, for emission emerging from any part of the bonding FS, Cu sites essentially do not contribute to the photointensity. In sharp contrast, contribution from O_{Cu} -sites in Fig. 3(b) is substantial. In fact, the remaining sites in the crystal lattice (not shown) are found to give little contribution, which explains why the intensity pattern from O_{Cu} -sites in Fig. 3(b) is quite similar to the corresponding total intensity in Fig. 2(a). Much of the preceding commentary concerning the bonding FS is

also seen to be valid for the antibonding FS by looking at Figs. 3(c), 3(d) and 2(b) and need not be repeated. The results of Fig. 3 thus substantially extend the observations made in Ref. 2 at a single \mathbf{k}_{\parallel} -value (i.e. $M(\pi, 0)$ point) to show that the ARPES matrix element is dominated by contribution from O_{Cu} -sites in the CuO_2 planes over the *entire FS* at photon energies below 25 eV. We have carried out limited computations at higher energies and find that around $h\nu = 40$ eV both Cu and O_{Cu} contribute roughly equally to the photointensity.

C. Why copper electrons do not contribute?

Eqs. 2 and 6 make it clear that the value of the momentum matrix element depends on the magnitudes and phases of several component quantities, namely, the expansion coefficients $C_L^{\gamma,\delta}$ of the initial and final states, the Gaunt coefficients $\mathcal{G}_{L,L'}^{\alpha}$, and the radial integral terms $B_{l,l'}^{\gamma,\delta}$. Concerning the character of the *initial states* of interest here, note that the antibonding as well as the bonding initial states in the vicinity of the FS in Bi2212 primarily consist of electrons in the CuO_2 bilayers, where the $O_{Cu,x}$, $O_{Cu,y}$ and Cu atomic sites contain approximately 80-90% of the weight in the associated Bloch wave function². The primary Cu orbital involved is $d_{x^2-y^2}$, while the most relevant O_{Cu} orbitals are p_x and p_y . The distribution of electrons between different sites and orbitals changes as a function of \mathbf{k}_{\parallel} , but in general the electrons at $E \approx E_F$ are strongly concentrated in the vicinity of the CuO_2 planes.

Since the initial states of interest are mainly Cu d and O_{Cu} p type, from various possible $L \rightarrow L'$ transition channels in Eq. 6, the dipole selection rule $\Delta l = \pm 1$ limits the L' for the *final states* to the Cu p and f states and O_{Cu} s and d states, respectively. A handle on the availability of appropriate final states (i.e. a substantial final state coefficient $C_{L'}^{\gamma,\delta}$) is provided by the partial densities of states (PDOS's) of the final states resolved into different l' -channels and sites, shown in panels (a)-(d) of Fig. 4. In the case of Cu, Figs. 4(a) and 4(b) show that PDOS is substantial only in the p channel, the value in the f channel being quite small, so that significant contribution to the matrix element is to be expected only from the $d \rightarrow p$ transitions. Similarly, Figs. 4(c) and 4(d) show that for the O_{Cu} -related final states, the d PDOS is substantial so that the $p \rightarrow d$ transitions from O_{Cu} -sites will dominate. In short, the lack of Cu f -type and O_{Cu} s -type final states in effect ‘‘blocks’’ the Cu $d \rightarrow f$ and O_{Cu} $p \rightarrow s$ channels in the allowed dipole transitions such that only Cu $d \rightarrow p$ and O_{Cu} $p \rightarrow d$ excitations remain to be of interest in further analysis.

We next consider the term $B_{l,l'}^{\gamma,\delta}$ of Eq. 6 which is defined by the radial integral of Eq. 3. This term may be thought of as the radial cross section associated with site (γ, δ) for the transition from l to l' orbital. In Fig. 4(e) these radial integrals are presented for the relevant Cu

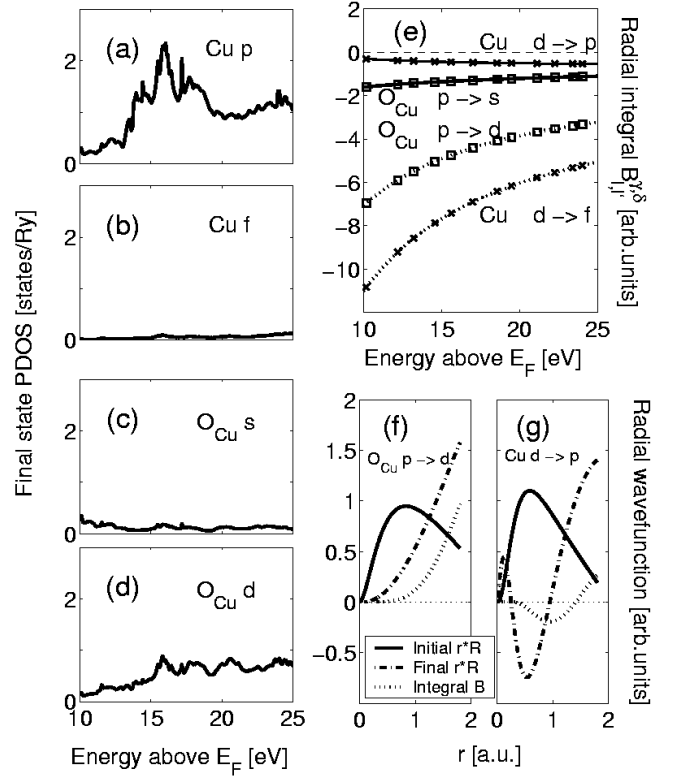


FIG. 4: Left-hand side: PDOS's for final states are presented as a function of energy above Fermi energy (E_F) for the most relevant angular momentum channels. (a) and (b) show the PDOSs of Cu p and f , and (c) and (d) show the O s and d final states. Right-hand side: (e) gives the radial integral term $B_{l,l'}^{\gamma,\delta}$ of Eq. 6 for indicated $l \rightarrow l'$ transitions from the bonding initial state at $\beta = 0^\circ$ (near M -point) as a function of final state energy. The data with crosses (squares) is for Cu (O_{Cu}) sites of the CuO_2 planes. In (f) and (g), typical initial (solid) and final (dash-dotted) state radial wave functions $R_l^\beta(r)$ and $R_{l'}^\beta(r)$, respectively, are shown as a function of radius r for O_{Cu} $p \rightarrow d$ and Cu $d \rightarrow p$ transitions, respectively. The dotted line shows the behavior of the radial overlap integral (Eq. 3).

and O_{Cu} related transitions. All curves are seen to be smooth, slowly varying functions of energy, although absolute values vary greatly between different transitions. The Cu $d \rightarrow f$ and O_{Cu} $p \rightarrow d$ excitation channels are the strongest, whereas the Cu $d \rightarrow p$ and O_{Cu} $p \rightarrow s$ integrals are smaller and will attenuate the related excitations. In view of the discussion of the preceding paragraph, weakness of the Cu $d \rightarrow p$ radial cross section is particularly important, since the Cu $d \rightarrow p$ channel is the only Cu transition channel that could have contributed substantially to the photointensity. It follows then that the O_{Cu} $p \rightarrow d$ is the main transition channel in the formation of the momentum matrix element for emission from the FS in Bi2212 at low photon energies.²⁹

Insight into the relative magnitudes of the O_{Cu} $p \rightarrow d$

and Cu $d \rightarrow p$ related radial cross sections can be gained by considering the behavior of initial and final state radial wave functions as shown in panels (f) and (g) of Fig. 4. In the case of $O_{Cu} p \rightarrow d$ transition, initial and final states in Fig. 4(f) are both nodeless and thus the integral $B_{l,l'}^{\gamma,\delta}$ does not change sign. By contrast, the wave function for the Cu p final state in Fig. 4(g) (dot-dashed) possesses two nodes so that when it is combined with the nodeless Cu d initial state radial wave function the integral oscillates in sign yielding a small value of the radial cross section for this transition. This mechanism where the nodes in the final state wave function play an important role is reminiscent of the arguments made in connection with the origin of the Cooper minima^{24,25,26} observed in photoionization cross sections of atomic systems at higher photon energies.³⁰ Putting it all together, the discussion of this section shows that even though the initial states at the FS in Bi2212 possess considerable Cu d character, these states contribute little to photointensity for $h\nu \leq 25$ eV due to a combination of two effects: The d to f channel is suppressed due to the lack of available f -type final states, while the d to p channel possesses a weak radial cross section.³¹

IV. SUMMARY AND CONCLUSIONS

We consider the nature of ARPES spectra from Bi2212 for emission from the Fermi energy. Over the 5-25 eV photon energy range, the spectra are shown to display remarkable spatial selectivity properties in the sense that emissions are dominated by excitation from just the O-sites in the CuO_2 planes, even though the initial state wave functions involved possess substantial Cu character. This selectivity applies to the bonding as well as the antibonding FS sheet and holds throughout the $(\mathbf{k}_x, \mathbf{k}_y)$ plane. Insight into the origin of this effect is obtained by considering the dipole matrix element for transitions between the relevant initial and final states and by decomposing this matrix element into contributions arising from individual sites in the unit cell in various angular momentum channels. Our analysis reveals that, of the two possible channels for exciting Cu d -electrons ($d \rightarrow f$ and $d \rightarrow p$), the $d \rightarrow f$ channel is suppressed by lack of available f -type final states, while the $d \rightarrow p$ channel is effectively blocked due to a small radial cross section

(i.e. the term $B_{l,l'}^{\gamma,\delta}$ in Eq. 6). Similarly, of the two possible channels for O p -electrons ($p \rightarrow s$ and $p \rightarrow d$), the $p \rightarrow s$ channel is suppressed since few s -type final states are available, leaving significant contribution to the spectrum from only the O $p \rightarrow d$ transitions. It turns out that the presence of nodes in the final state wave function tends to reduce the radial cross section, which is reminiscent of Cooper minimum type effect in photoionization cross section of atomic systems. Limited computations at higher photon energies show that the contribution from Cu sites increases at higher energies, and that by around 40 eV, the Cu and O states are excited roughly equally in the spectrum.

Our prediction that ARPES can preferentially sample Cu or O states by tuning the photon energy suggests novel possibilities for exploiting energy dependent ARPES spectra for probing initial state characters. An exciting example in the cuprates would be to test the Zhang-Rice mechanism^{11,12} and potentially to deduce experimentally the value of the Hubbard U parameter as a function of doping. Zhang and Rice noted that large U greatly restricts double occupancy of Cu orbitals, so that the first holes doped at near half filling – equivalently, the states at the top (high energy part) of the lower Hubbard band – should have strong O character. Thus, even though ARPES cannot see the upper Hubbard band (and hence cannot measure U directly), it should be possible to adduce U by measuring the relative Cu/O character of states along the lower Hubbard band, and comparing this to predictions of appropriate model computations. A direct determination of the doping dependence of U would be an important confirmation of recent results and predictions¹³.

Acknowledgments

It is a pleasure to acknowledge important discussions with Bob Markiewicz. This work is supported by the US Department of Energy contract DE-AC03-76SF00098, and benefited from the allocation of supercomputer time at NERSC, Northeastern University's Advanced Scientific Computation Center (ASCC) and the Institute of Advanced Computing (IAC), Tampere. One of us (S.S.) acknowledges Suomen Akatemia and Vilho, Yrjö ja Kalle Väisälän Rahasto for financial support.

¹ A. Bansil and M. Lindroos, Phys. Rev. Lett. **83**, 5154 (1999).

² M. Lindroos, S. Sahrakorpi and A. Bansil, Phys. Rev. B **65**, 054514 (2002).

³ A. Bansil, M. Lindroos, S. Sahrakorpi, R. S. Markiewicz, G. D. Gu, J. Avila, L. Roca, A. Tejada and M. C. Asensio, J. Phys. Chem. Solids **63**, 2175 (2002).

⁴ M. C. Asensio, J. Avila, L. Roca, A. Tejada, G.D. Gu, M. Lindroos, R. S. Markiewicz and A. Bansil, Phys. Rev. B

67, 014519 (2003).

⁵ Y.-D. Chuang, A. D. Gromko, A.V. Fedorov, Y. Aiura, K. Oka, Y. Ando, M. Lindroos, R. S. Markiewicz, A. Bansil and D. S. Dessau, Submitted to Phys. Rev. B (2003).

⁶ D. L. Feng, C. Kim, H. Eisaki, D. H. Lu, A. Damascelli, K. M. Shen, F. Ronning, N. P. Armitage, N. Kaneko, M. Greven, J.-i. Shimoyama, K. Kishio, R. Yoshizaki, G. D. Gu and Z.-X. Shen, Phys. Rev. B **65**, 220501(R) (2002).

⁷ A. A. Kordyuk, S. V. Borisenko, T. K. Kim, K. A. Nenkov,

- M. Knupfer, J. Fink, M. S. Golden, H. Berger, and R. Follath, Phys. Rev. Lett. **89**, 077003 (2002).
- ⁸ A. Damascelli, Z.-X. Shen and Z. Hussain, cond-mat/0208504 (2002).
- ⁹ J. C. Campuzano, M. R. Norman and M. Randeria, cond-mat/0209476 (2002).
- ¹⁰ I. Vekhter and C. M. Varma, cond-mat/0210508 (2002).
- ¹¹ F.C. Zhang and T.M. Rice, Phys. Rev. B **37**, 3759 (1988).
- ¹² Y. Harada, K. Okada, R. Eguchi, A. Kotani, H. Takagi, T. Takeuchi, and S. Shin, Phys. Rev. B **66**, 165104 (2002).
- ¹³ C. Kusko, R.S. Markiewicz, M. Lindroos, and A. Bansil, Phys. Rev. B **66**, 140513(R) (2002).
- ¹⁴ K. Gofron, J. C. Campuzano, A. A. Abrikosov, M. Lindroos, A. Bansil, H. Ding, D. Koelling, and B. Dabrowski, Phys. Rev. Lett. **73**, 3302 (1994).
- ¹⁵ M. Lindroos and A. Bansil, Phys. Rev. Lett. **75**, 1182 (1995).
- ¹⁶ A. Bansil and M. Lindroos, J. Phys. Chem. Solids **56**, 1855 (1995).
- ¹⁷ M. Lindroos and A. Bansil, Phys. Rev. Lett. **77**, 2985 (1996).
- ¹⁸ S. Sahrakorpi, Ph.D. Thesis, Tampere University of Technology, Publications 354 (2001).
- ¹⁹ S. Sahrakorpi, M. Lindroos and A. Bansil, Phys. Rev. B **66**, 235107 (2002).
- ²⁰ P. E. Mijnders and A. Bansil, J. Phys.: Condens. Matter **2**, 911 (1990).
- ²¹ See, e.g., A. Bansil, S. Kaprzyk, P. E. Mijnders and J. Tobola, Phys. Rev. B **60**, 13396 (1999), and references therein.
- ²² A. B. Chen, Phys. Rev. B **14**, 2384 (1976).
- ²³ P. V. Bogdanov, A. Lanzara, X. J. Zhou, S. A. Kellar, D. L. Feng, E. D. Lu, H. Eisaki, J.-I. Shimoyama, K. Kishio, Z. Hussain and Z. X. Shen, Phys. Rev. B **64**, 180505(R) (2001).
- ²⁴ J. W. Cooper, Phys. Rev. **128**, 681 (1962).
- ²⁵ J. J. Yeh and I. Lindau, At. Data Nucl. Data Tables **32**, 1 (1985).
- ²⁶ S. L. Molodtsov, S. V. Halilov, V. D. P. Servedio, W. Schneider, S. Danzenbächer, J. J. Hinarejos, M. Richter and C. Laubschat, Phys. Rev. Lett. **85**, 4184 (2000).
- ²⁷ The site selectivity effect discussed in this article was noted in Ref. 2. However, Ref. 2 considered only a single \mathbf{k}_{\parallel} -point, namely the $M(\pi, 0)$ symmetry point and did not attempt to elucidate the origin of this effect in terms of radial cross sections, etc. as done in this study.
- ²⁸ This bulk momentum matrix element of course does not take into account effects of surface termination, the finite lifetimes of the initial and final states, etc.
- ²⁹ P. Marksteiner et al., Phys. Rev. B **38**, 5098 (1988), considered angle-integrated photointensities and found that the spectra are weighted in favor of Cu excitations at higher photon energies.
- ³⁰ According to J. J. Yeh and I. Lindau, Ref. 25, the atomic photoionization cross section is approximately one third smaller for the Cu $3d$ than for the O $2p$ atomic levels at photon energies around 30 eV.
- ³¹ The destructive interference discussed in Ref. 2 between Cu terms of different CuO_2 -planes decreases the Cu-related intensity further. This destructive interference seems to be more prevalent for the Cu terms than for the O_{Cu} -terms.